International Journal of Heat and Fluid Flow 30 (2009) 1106–1113

Contents lists available at ScienceDirect

International Journal of Heat and Fluid Flow

journal homepage: www.elsevier.com/locate/ijhff

Study on the radial jet velocity distribution of two closely spaced opposed jets

Zhi-Gang Sun, Wei-Feng Li, Hai-Feng Liu *

Key Laboratory of Coal Gasification of Ministry of Education, East China University of Science and Technology, Shanghai 200237, PR China

ARTICLE INFO

Article history:
Received 31 March 2009
Received in revised form 15 September 2009
Accepted 15 September 2009

Keywords:
Two opposed jets
Small nozzle separation
Radial jet
Turbulence
Hot-wire anemometer

ABSTRACT

The experimental and theoretical researches on the radial jet of two opposed jets have been carried out in this paper. The radial velocities of opposed jets with various exit velocities, nozzle diameters and nozzle separations were measured experimentally by a hot-wire anemometer (HWA). The results show that, the normalized radial velocities are self-similar across various radial sections at $r \geqslant 1.5D$ and the radial velocity profiles can be described by a Gaussian distribution function. The half-width increases linearly with increasing radial distance at $r \geqslant 1.5D$, and spreading rates of radial jet are about 0.121. The normalized radial velocity at impingement plane increases firstly, and then decreases with the increasing normalized radial distance. The normalized radial velocity is independent on nozzle diameter, nozzle separation and exit velocity. The maximum radial velocity at impingement plane is proportional to the exit velocity, and it is inversely proportional to the 0.551th power of the normalized nozzle separation. The position of the maximum radial velocity increases with the nozzle separation at $L/D < 1$, and keeps invariant at $L/D \geqslant 1$.

1. Introduction

Due to rapid and high-effective mixing performance, opposed jets have been studied experimentally (Stan and Johnson, 2001; Lindstedt et al., 2005) and theoretically (Champion and lippy, 1993; Bray et al., 1992) over many years. It has also been widely used in a number of industrial applications including coal gasification (Wang et al., 2007), mixing (Santos et al., 2005), absorption (Berman et al., 2000), liquid–liquid extraction (Dehkordi, 2002), drying (Hosseinalipour and Mujumda, 1995), etc. The radial jets of opposed jets are of importance in many applications such as ventilating ducts, internal combustion engine valves, and turbine-blade cooling techniques (Witze and Dwyer, 1976; Hunt and Ingham, 1992), etc.

A number of authors have studied various aspects of the radial jet from two closely spaced parallel circular discs. The earliest theoretical treatment of the radial jet appears to have been done by Rumer (1949), who performed a mixing-length analysis analogous two Tollmein's plane-jet solution. Schwarz (1963), Rajaratnam (1976) and Hunt and Ingham (1998) have theoretically studied the laminar and turbulent radial jets. Heskestad (1966) used a hot-wire anemometer to measure both the mean velocity and turbulence quantities, including lateral distributions of the normal and Reynolds stresses, and the intermittency factor of the radial jet with a fixed exit velocity and nozzle separation. Witze and Dwyer (1976) have investigated the mean velocity and turbulence intensity distributions in turbulent radial jets. In their investigation, the radial jets were classified as "constrained radial jets" and "impinged radial jets". They researched the lateral profile data, the half-width, the virtual origin, the centre-line mean velocity and turbulence data. Tanaka and Tanaka (1976) studied the mean velocity and turbulence together with pressure distributions in the radial jets flows by changing diameter and width of nozzles and exit velocity. They used three types of nozzles to find the effects of the nozzle shape on the radial jet flow, however the normalized nozzle separations were very small. Patel (1979) researched the normalized mean velocity profiles, the growth and the variation of centre-line velocities of the radial free jet which produced by two very small spaces identical and opposing impinging jets. The turbulent radial jet has also been studied by Wood and Chen (1985), who described results of a numerical investigation. They made comparisons between three different turbulence models and the experimental results of Heskestad (1966). Rubel (1985) has examined the applicability of various k–ε turbulence models to the radial jet by comparing the spreading rate of the radial jet predicted by the models with those determined from experiment. But all above studies are concentrated in the radial jet with very small nozzle separations.

However, as the normalized nozzle separations become larger, the researches on the radial jet produced by opposed jets are still very limited. Several radial velocities were researched in the stagnation region of $L/D = 0.2$–2. Champion and Lippy (1991, 1993) studied two closely spaced opposed jets on the basis of a Reynolds stress theory. In their work, the mean axial and radial velocity, the intensities have been researched. Korusoy and Whitelaw (2001)

* Corresponding author. Tel.: +86 21 64251418; fax: +86 21 64251312.
E-mail address: hfliu@ecust.edu.cn (H.-F. Liu).

0142-727X/$ - see front matter © 2009 Elsevier Inc. All rights reserved.
doi:10.1016/j.ijheatfluidflow.2009.09.003

Notations

$b_{1/2}$	the half-width, mm	u_{rms}	the root mean square velocities, m/s
D	the nozzle diameter, mm	$u_{r,\max}$	the maximum radial velocity at impingement plane, m/s
L	the nozzle separation, mm	$u_{r,\mathrm{rms}}$	the root mean square velocities at impingement plane, m/s
Re	the exit Reynolds number	r_{m}	the distance from the maximum radial velocity to the stagnation point, mm
u_0	the exit air velocity, m/s	τ_w	wall shear stress, Pa
u_x	the axial velocity, m/s	v	kinematical viscosity, m^2/s
u_r	the radial velocity, m/s		
$u_{r,\mathrm{m}}$	the radial velocity at impingement plane, m/s		

studied the pressure distributions, the axial and radial velocity distributions, and the mean strain rate of opposed jets with small separations by static pressure probe, HWA and LDV. The radial velocity was directly proportional to the bulk velocity in the impingement region. The radial position of the peak and the amplitude in radial velocity increased as the separation was reduced. Kostiuk et al. (1993) studied the velocity distribution of opposed jets using LDV. The mean flow was found to be self-similar for all the conditions tested, and produced a region of plane straining which was homogeneous in the vicinity of the stagnation. However, the above studies are concentrated in the impingement region.

From above studies, we know that the researches on the radial jets are mainly "constrained radial jets" with very small normalized nozzle separations ($L/D < 0.13$) and "impinged radial jets" with large nozzle separations ($L/D > 16$). When the nozzle separation is very small, the radial jets are just like the "constrained radial jets" and the nozzle shape has great influence on the flow structure. Our previous study (Li et al., 2008) has found that the stagnation point offset was unstable at the middle nozzle separation ($2 < L/D < 12$). In this region, it is extremely difficult to make the stagnation plane stay stably at the middle of the two nozzles, therefore the radial jet produced by the opposed jet is also unstable. So in this paper, we perform theoretical analysis and experimental studies on the radial jets produced by two closely spaced turbulent opposed jets at $0.17 \leqslant L/D \leqslant 2$. Our objectives are to: (a) research the radial velocity characteristic of the radial jet and (b) identify the effects of the nozzle separation, nozzle diameter and exit air velocity on the radial jet by experimental measurements.

The remainder of this paper is organized as follows: the experiment setup is introduced in the following Section 2. The theoretical analysis of the radial jet is deduced in Section 3. Results and discussion are presented in Section 4. The paper ends with the conclusion in Section 5.

2. Experimental apparatus and procedure

Fig. 1 shows the apparatus to produce opposed jets in our experiment. The air coming from roots blower (1) were controlled by two valves (2) and the flow rates were measured by two flowmeters (3), respectively. Then the air entered two coaxial and opposed nozzles (5) having the same configuration as plotted in Fig. 2. When two fluid elements which have same velocity and reversed flow direction impinge, the stagnation point and the radial flow are formed, as shown in Fig. 3. In Fig. 3, r denotes the radial distance from the stagnation point, u_r is the radial velocity of the

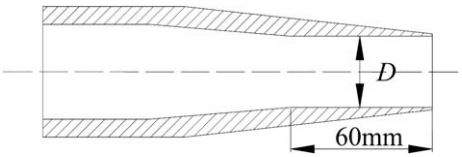

Fig. 2. Cross section of the nozzle.

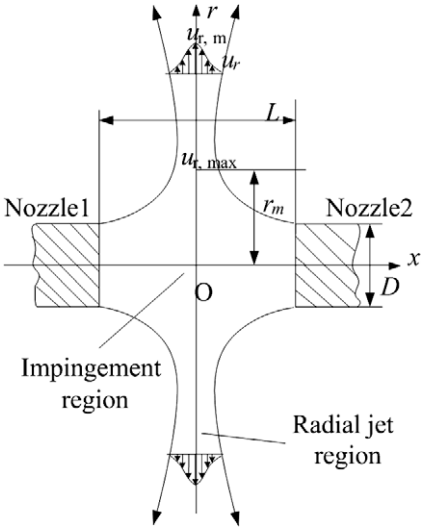

Fig. 3. Schematic map of the radial jet.

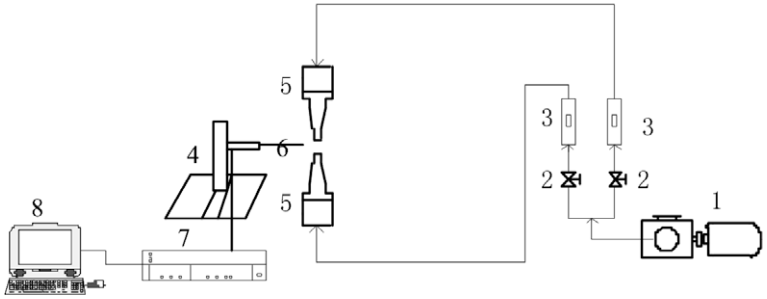

Fig. 1. The flow chart of the experiment.

Table 1
The measurement cases.

D (mm)	***L*** (mm)	***Re***
10	5, 10, 15, 20	8200–32,800
20	5, 10, 15, 20, 30, 40	16,400–65,600
30	5, 10, 15, 20, 30, 45, 60	12,300–98,400

radial jet alone r direction, $u_{r,\mathrm{m}}$ is the radial velocity of the radial jet at $x = 0$ plane, and $u_{r,\max}$ is the maximum radial velocity at $x = 0$ plane. L is the nozzle separation and r_{m} is the distance from the position with maximum radial velocity to the stagnation point. It can be seen that the radial jet is a radially outward plane flux of fluid which develops along the direction r.

In this paper, the radial velocity of the radial jet was measured by the DANTEC hot-wire anemometer, which is similar to Heskestad (1966), Tanaka and Tanaka (1976), Witze and Dwyer (1976) and Korusoy and Whitelaw (2001). The hot-wire can not provide correct measurements of the radial velocities close to the axis where the mean velocities were low and the fluctuation levels finite, But the hot-wire can be used to measure the radial velocities of the radial jet, because the axial velocities are very small in the impingement region and the radial jet region. The radial velocities measurements with the laser-Doppler anemometer agreed with the hot-wire in Korusoy and Whitelaw (2001). The probe has a single wire. The sampling frequency of the system was 20 kHz, and the sampling time was 10 s. In order to control the measured point precisely, the HWA probe was mounted on a traverse system which can adjust the coordinate up to 0.1 mm. Based on the results of Kawall et al. (1983), the maximum hot-wire measurement error was evaluated to be less than 5% and is attributed to the high turbulent intensities in the separated shear layer and near wake. The reproducibility of the measurements of mean radial velocity at the stagnation plane was determined by repeating a point measurement ten times, which yielded a standard deviation of 3%.

In this paper, the radial velocity of the radial jet produced by the closely spaced opposed jet was experimentally studied at various nozzle separations, nozzle diameters and exit air velocities. The detailed measurement cases are listed in Table 1. The jet Reynolds number at the nozzle exit is defined as:

$$Re = \frac{Du_0\rho}{\mu}, \tag{1}$$

where D is the nozzle diameter, u_0 is the bulk velocity of the jet at the nozzle exit, ρ and μ are the density and the dynamic viscosity of air under normal conditions. It can be seen that the flow is in turbulence state from Table 1.

3. The velocity characteristic

We consider the cylindrical coordinate shown in Fig. 3 with coordinates x, r and with associated velocity components u_x and u_r. The velocity field is both axisymmetric about the axis of the two nozzles and symmetric about the $x = 0$ plane i.e. the impingement plane.

The equations of motion for the radial turbulence jet involving sufficiently high turbulence Reynolds numbers such that the molecular transport may be neglected are (White, 2004)

$$\overline{u_r}\frac{\partial \overline{u_r}}{\partial r} + \overline{u_x}\frac{\partial \overline{u_r}}{\partial x} = -\frac{1}{\rho}\frac{\partial \overline{\rho u_x' u_r'}}{\partial x} - \nu\frac{\partial^2 \overline{u_r}}{\partial x^2}; \tag{2}$$

$$\frac{\partial r\overline{u_r}}{\partial r} + \frac{\partial r\overline{u_x}}{\partial x} = 0. \tag{3}$$

The boundary conditions satisfied the velocity field are

$$u_x = 0; \quad u_r = u_{\mathrm{m}}; \quad \frac{\partial v_r}{\partial x} = 0; \quad \text{at } x = 0,$$
$$u_r = 0; \quad \text{at } x = \infty.$$

Multiply Eq. (2) by r, and integrate it, and the integrated lower and upper limit is x and ∞, then we obtain

$$\frac{\partial}{\partial r}\int_x^\infty r u_r^2 dx - r u_x u_r - r\overline{u_x' u_r'} - \nu r\frac{\partial u_r}{\partial x} = 0. \tag{4}$$

The velocity distribution and turbulent shear stress distributions are self-similar for radial jet, so the radial velocity and the wall shear stress are expressed as:

$$u_r/u_{r,\mathrm{m}} = f(\eta), \tag{5}$$

$$\frac{\tau_w}{\rho u_{r,\mathrm{m}}^2} = -\frac{\rho\overline{u_x' u_r'}}{\rho u_{r,\mathrm{m}}^2} = g(\eta), \tag{6}$$

where $\eta = x/b$, and $u_{r,\mathrm{m}}$, b are the velocity scale and length scale, respectively, which are only associated with the variable r.

The mean axial velocity is 0 at $x = 0$. Integrate Continuity Equation, and u_x can be derived as:

$$u_x = -\frac{b u_{r,\mathrm{m}}}{r}\int_0^\eta f d\eta - b\frac{du_{r,\mathrm{m}}}{dr}\int_0^\eta f d\eta + u_{r,\mathrm{m}}\frac{db}{dr}\int_0^\eta \eta\frac{df}{d\eta}d\eta. \tag{7}$$

Substitution Eqs. (5)–(7) into Eq. (4), and obtain the equation

$$-\frac{r}{b}\frac{db}{dr}\eta f\frac{df}{d\eta} + \frac{r}{u_{r,\mathrm{m}}}\frac{du_{r,\mathrm{m}}}{dr}f^2 + \frac{r}{b}\frac{db}{dr}\frac{df}{d\eta}\int_0^\eta \eta\frac{df}{d\eta}d\eta - \frac{r}{u_{r,\mathrm{m}}}\frac{du_{r,\mathrm{m}}}{dr}\frac{df}{d\eta}\int_0^\eta f d\eta - \frac{df}{d\eta}\int_0^\eta f d\eta + \frac{r}{b}\frac{u_{r,\mathrm{m}}^2}{u_{r,\mathrm{m}}^2}\frac{dg}{d\eta} = 0. \tag{8}$$

If the flow is self-similar, the Eq. (8) which is associated with f and g is independent on r. Such that normalized groups:

$$\frac{r}{b}\frac{db}{dr}; \quad \frac{r}{u_{r,\mathrm{m}}}\frac{du_{r,\mathrm{m}}}{dr}; \quad \frac{r}{b}\frac{u_{r,\mathrm{m}}^2}{u_{r,\mathrm{m}}^2} \tag{9}$$

are 0 or const. Then, $u_{r,\mathrm{m}}$ and b are dependent on the power of r from Eq. (9),

$$u_{r,\mathrm{m}} = Mr^m; \quad b = Nr. \tag{10}$$

It indicates that the radial velocity of the radial jet at impingement plane changes exponentially with the radial distance r, and the jet width is proportional to r.

4. Experimental results

4.1. The velocity distribution at the nozzle exit

The measured normalized axial mean velocity and root mean square velocity (u_{rms}) profiles at the exit of a single nozzle are shown in Fig. 4. It is seen that the nozzles in this experiment have top-hat exit velocity profiles and mean velocity profiles are flat for about 80% of the nozzle diameter D and the thickness of the boundary layer is about $0.1D$. The normalized rms velocities are about 5% except the region within $0.1D$ close to the nozzle wall.

4.2. The lateral profile and the half-width

Fig. 5 shows the distributions of velocities $u_r/u_{r,\mathrm{m}}$ and turbulence u_{rms}/u_r across the sections at $r/D = 0.75$ to 10, respectively. It can be found that the radial velocities are flat at $r/D = 0.75$ and 1.0, and the region which has equal velocity decrease with the increasing radial distance. The radial velocities are self-similar across the sections at $r/D \geqslant 1.5$.

The turbulence intensities increase firstly, and then decrease with the increasing lateral distance. The values along the centre-

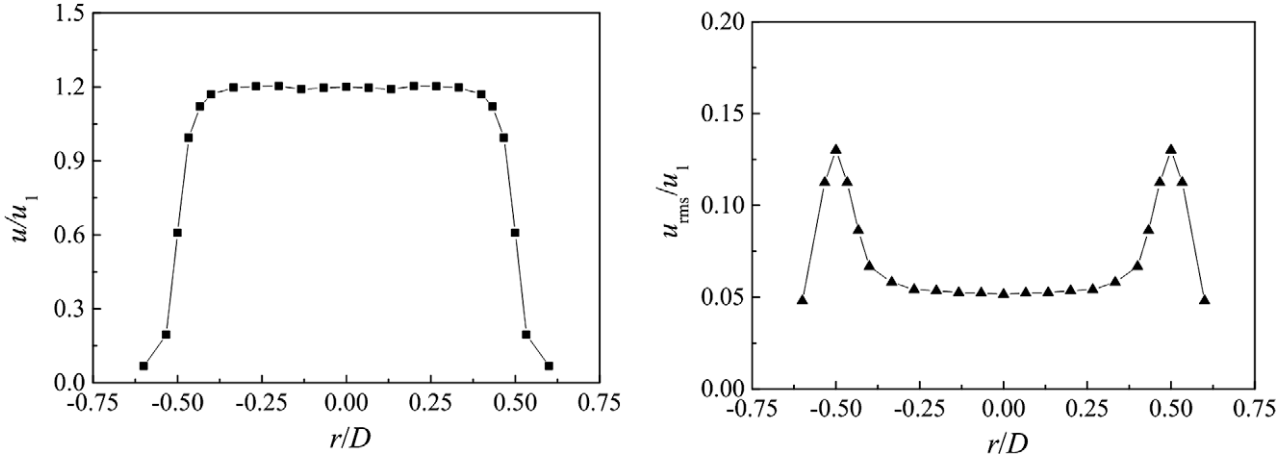

Fig. 4. Distributions of normalized axial mean and rms velocities at the exit of the free jet.

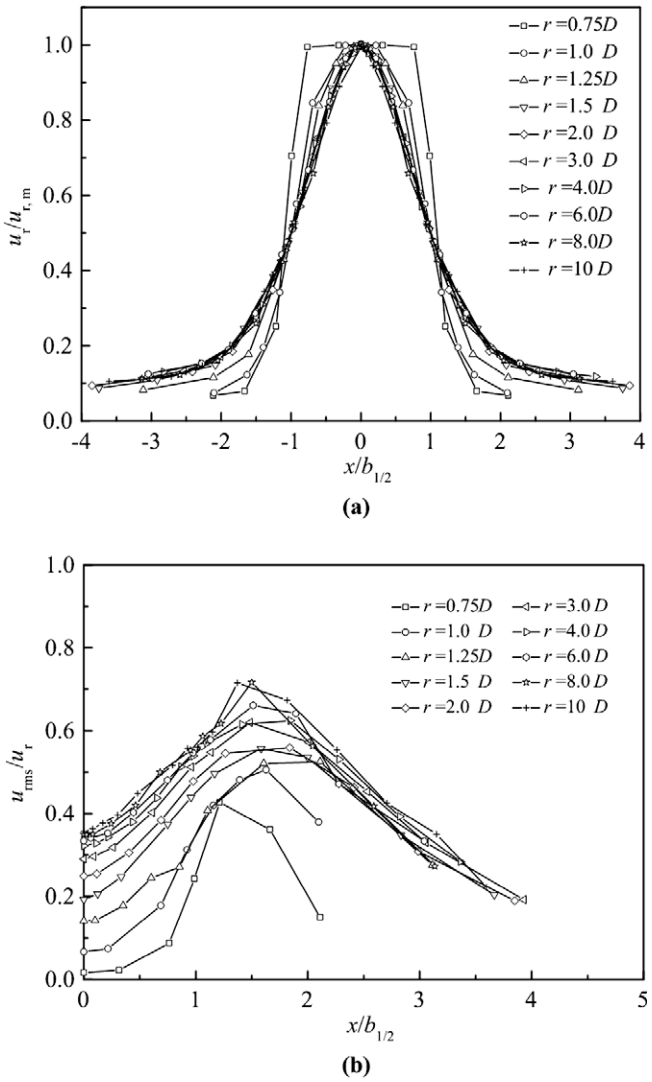

Fig. 5. The lateral distributions of velocities and turbulences (D = 20 mm, L = 0.5D, u_0 = 23.6 m/s).

line at $x/b_{1/2} = 0$ indicate that self-preservation of the turbulence intensities is not achieved since u_{rms}/u_r at stagnation plane is not constant. The turbulence intensities increase with the increasing radial distance. The differences in turbulence intensities at $r/D \geqslant 4$ are small, and turbulence intensities reach the maximum of 0.6–0.7 about at $x/b_{1/2} = 1.6$.

The radial velocity distributions at various sections at $r/D \geqslant 1.5$, D = 10, 20, 30 mm, u_0 = 23.6 m/s and various nozzle separations are shown in Fig. 6, in which the results are compared with the self-similar velocity profile given by Eqs. (11) and (12). The measured values are clearly self-similar across various sections at $r/D \geqslant 1.5$ for all experimental cases, just as the free jet. The velocity distribution characterizes as Gaussian distribution which is maximum at the impingement plane and decreases with the increasing lateral distance. The radial velocity is expressed as:

$$\frac{u_r}{u_{r,\mathrm{m}}} = \exp\left\{-k \times \left(\frac{x}{b_{1/2}}\right)^2\right\}, \quad k = 0.69, \quad \text{for } \frac{x}{b_{1/2}} < 1.5, \tag{11}$$

where $b_{1/2}$ is the half-width i.e. the vertical distance of the position with $u_r = 0.5u_{r,\mathrm{m}}$ to the impingement plane, and k is the empirical constant, which is the same as the free jet. The uncertainty in the calculation by Eq. (11) is 3.5%. The absolute error increases with the increasing x.

The results are also in good agreement with the following equation proposed by Tanaka and Tanaka (1976):

$$\frac{u_r}{u_{r,\mathrm{m}}} = 1 - \tanh^2\left(\frac{0.881x}{b_{1/2}}\right), \quad \text{for } \frac{x}{b_{1/2}} < 1.5. \tag{12}$$

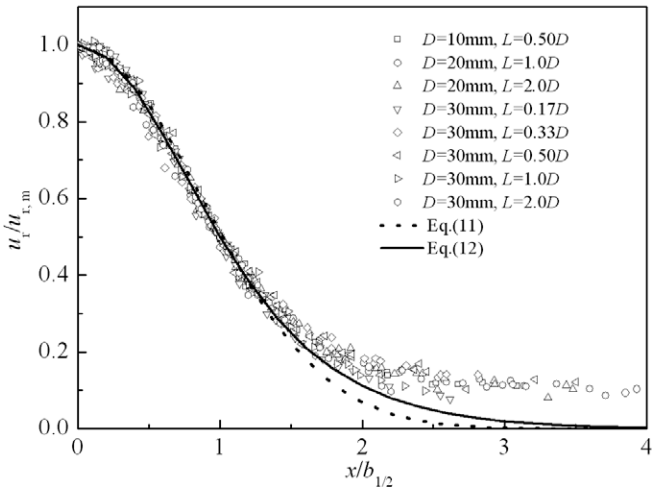

Fig. 6. The radial velocity distribution across various sections at $r/D \geqslant 1.5$.

The uncertainty in the calculation by Eq. (12) is 2.9%. But both equations underpredict the experimental values at $x/b_{1/2} > 1.5$.

Fig. 7 shows the normalized half-widths at various exit velocities, nozzle diameters and normalized nozzle separations. The half-widths are invariable at $u_0 = 5.75$–23.0 m/s as shown in Fig. 7a, and the normalized half-widths change slightly with the increasing nozzle diameters from $D = 10$ mm to $D = 30$ mm, as shown in Fig. 7b. Fig. 7c shows that the half-widths increase slowly with the increasing normalized nozzle separations which are same as the constrained radial jet mentioned in Witze and Dwyer (1976).

A more certain indicator of self-similar is the linearity of the jet half-width. From Fig. 7, we can find that the half-widths are invariable, even the half-widths decrease with the increasing r/D from 0.75 to 1.5. The half-widths increase linearly with the increasing radial distance at $r/D \geqslant 1.5$. This indicates that the radial jet is self-similar at $r/D \geqslant 1.5$ for all experimental cases, which is same as the conclusion from velocity profile data.

The half-width values can be fit as:

$$\frac{b_{1/2}}{D} = 0.121\frac{r}{D}, \quad \text{for } r/D \geqslant 1.5. \tag{13}$$

This is in agreement with Eq. (10). The uncertainty in the calculation by Eq. (13) is 8.2%. This shows that the virtual origin locates at the stagnation point and the spreading rate is 0.121. And the spreading rate is independent of exit velocities, nozzle separations and nozzle diameters within current experimental cases. The spreading rate in Tanaka and Tanaka (1976) is about 0.967 and it is independent of nozzle separation and nozzle diameter at $D = 60$–120 mm and $L/D < 0.1$. Meanwhile the spreading rates are in the region of 0.106–0.16 for constrained radial jet of $0.001 < L/D < 0.12$ in Witze and Dwyer (1976). The difference may be caused by the difference in the nozzle configuration and the nozzle separation.

4.3. The radial velocity and turbulence at impingement plane

The normalized radial velocities along radial jet at stagnation plane at various nozzle separations are shown in Fig. 8. In Fig. 8a, the velocity is normalized by exit air velocity u_0 and the radial distance is normalized by nozzle diameter D. It can be seen that the maximum radial velocity ($u_{r,\max}$) at impingement plane decreases with the increasing nozzle separations. The radial velocity increases at $r < r_m$, and decreases at $r > r_m$ with the increasing radial distance. The radial velocity decreases at the radial distance with the increasing nozzle separations for opposed jets with equal exit velocities.

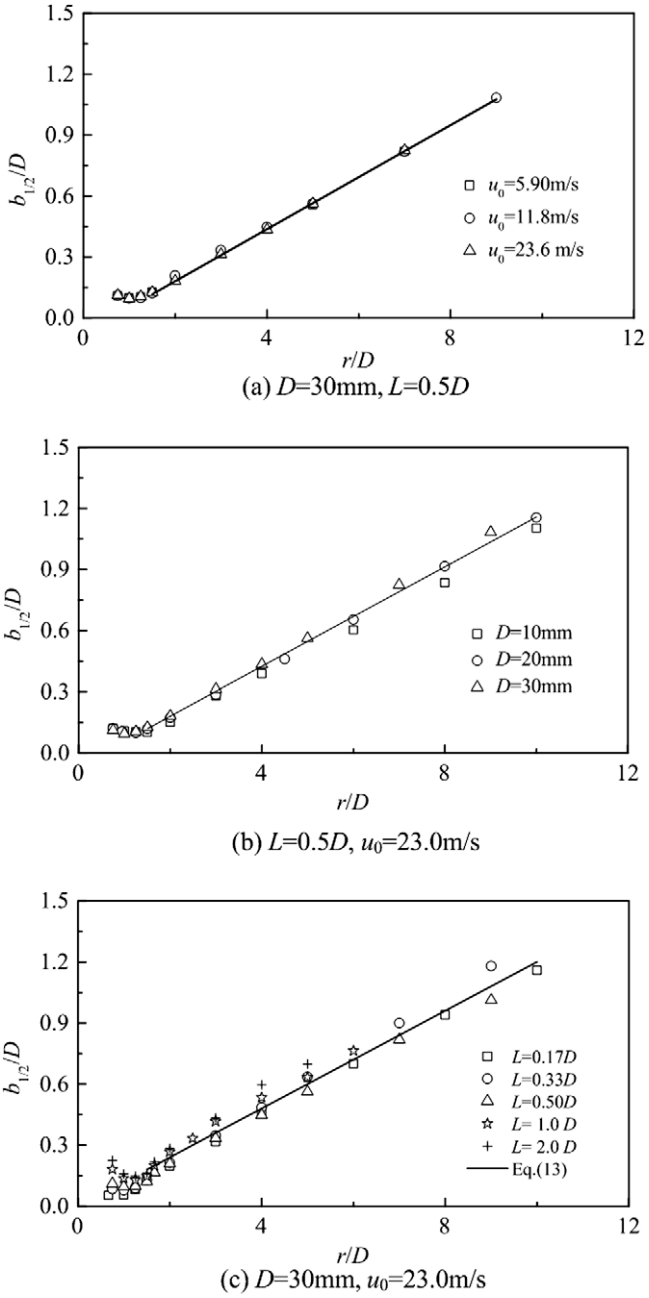

Fig. 7. Radial jet half-widths at various u_0, D and L/D.

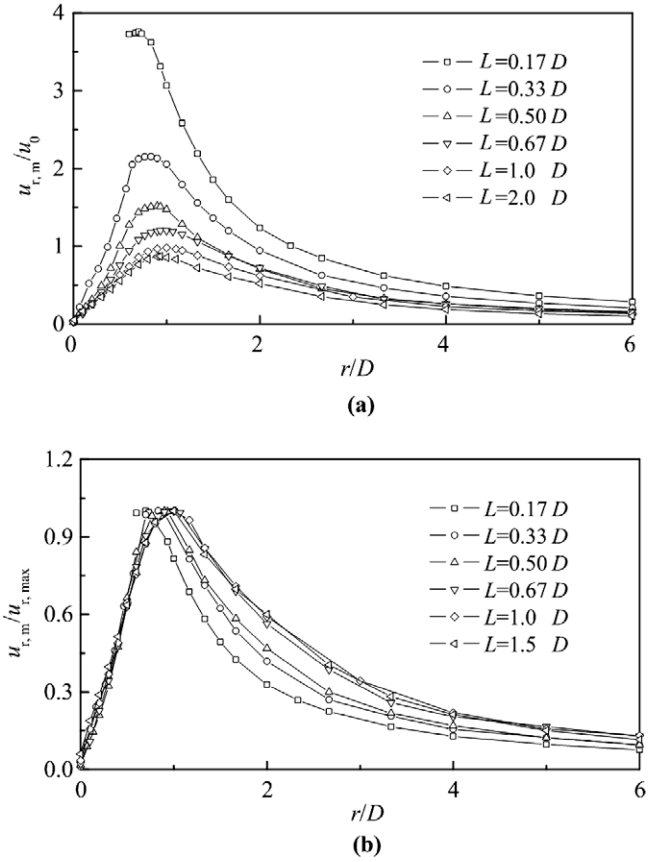

Fig. 8. The normalize radial velocity at impingement plane ($D = 30$ mm, $u_0 = 23.6$ m/s).

In Fig. 8b, the velocity is normalized by $u_{r,max}$ and the radial distance is normalized by nozzle diameter. It can be seen that, r_m decreases with the decreasing nozzle separations. The normalized radial velocity ($u_r/u_{r,max}$) decreases with the decreasing nozzle separations (L/D) at the same radial distance for $r > r_m$.

The radial velocities normalized by $u_{r,max}$ at different exit air velocity and $L = 0.5D$, $D = 20$ mm, 30 mm are shown in Fig. 9. The radial velocity distributions are the same as each other at different exit air velocity. The radial velocities at impingement plane ($u_{r,m}$) are proportional to the exit velocity and the maximum radial velocity position (r_m) is independent to exit velocity. From Section 4.2, we know that the lateral velocity distributions and the half-widths are almost the same at various exit velocity. Tamir (1994) has found that the axial velocity was proportion to u_0 and pressure was proportion to u_0^2. So the flow and pressure structures are invariable at different exit velocity. It can explain why r_m is independent to exit velocity.

The normalized radial velocities at various nozzle separations, $D = 10$, 20, 30 mm and $u_0 = 23.6$ m/s are shown in Fig. 10. The velocity is normalized by $u_{r,max}$ and the radial distance is normalized by r_m. It can be seen that, the nozzle separation and the nozzle diameter have no influence on the normalized radial velocities. The normalized radial velocities are self-similar and only correlated with the normalized radial distance. For two opposed jets, the axial flow translates to radial flow after the flow impinges to each other. At the radial position r_1, the radial velocity is mainly influenced by three factors. Firstly, the fluid at $r < r_1$ will flow through the position r_1 to the outer before the fluid changes direction completely. Secondly, the flow area shrinks due to the fluid axial flow inertia at the initial stage of changing direction. Thirdly, the radial jet boundary layer becomes thick due to the entrainment of the jet as the radial jet develops; meanwhile the flow area and the flow rate become large, which make the flow velocity decrease. The interaction of the above factors makes the radial jet velocity present a maximum when the flow area reaches the minimum at $r = r_m$. So the radial velocity first increases with the increasing radial distance at $r < r_m$, and it decreases with the increasing radial distance at $r > r_m$.

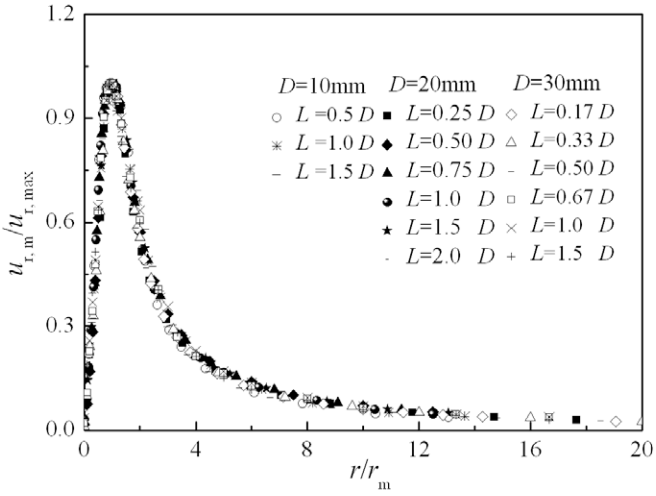

Fig. 10. The normalized radial velocity at impingement plane ($u_0 = 23.6$ m/s).

The half-widths in the region of $0.75 \leqslant r/D \leqslant 1.25$ change slightly which indicates that the flow area change slightly too, and in this region the axial flow have changed to radial flow completely, so the radial velocity at $0.75 \leqslant r/D \leqslant 1.25$ is close to the maximum radial velocity $u_{r,max}$, as shown in Fig. 8. According to the results of lateral velocity profiles, half-widths and the radial jet velocities at impingement plane, it can be concluded that, the radial jets are completely self-similar for $r/D > 1.5$. That is, the flow could be considered a fully developed radial jet and the profiles become self-similar for $r/D > 1.5$. And L/D and Re have no obvious influence on the distance where the profiles become self-similar for all cases in Table 1.

The normalized radial velocities at $r < 0.8r_m$ are shown in Fig. 11. It can be seen that the normalized radial velocities increase linearly with the increasing normalized radial distance before they reach maximum at various nozzle diameters and nozzle separations. The radial velocity is close to the maximum radial velocity at $r = 0.78r_m$. The experimental results in this paper can be fit as:

$$\frac{u_{r,m}}{u_{r,max}} = 1.26\frac{r}{r_m}, \quad \text{for } r < 0.78r_m. \tag{14}$$

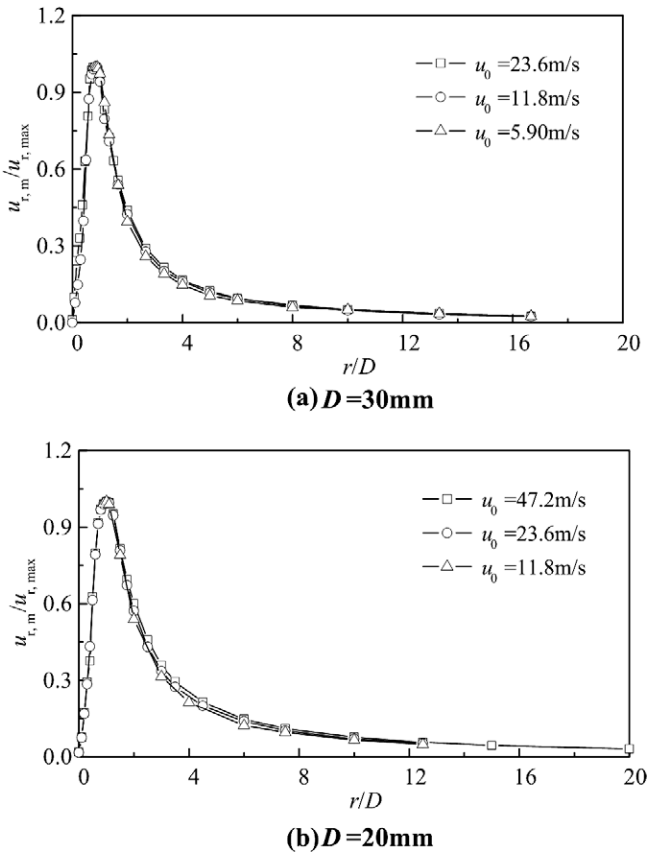

Fig. 9. The normalize radial velocity at various exit air velocities ($L = 0.5D$).

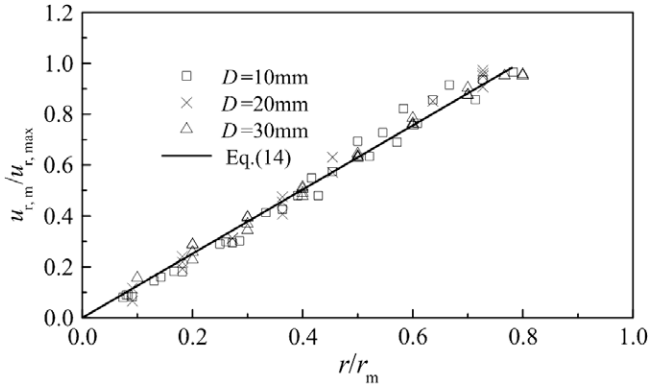

Fig. 11. The normalized radial velocity at impingement plane for $r < r_m$ ($u_0 = 23.6$ m/s).

The uncertainty in the calculation by Eq. (14) is 6.2%.

The normalized radial experimental velocity values at $r > 1.25r_m$ compared with the literature data from Heskestad (1966), Tanaka and Tanaka (1976), Witze and Dwyer (1976) and the fitting results by Eq. (15) are shown in Fig. 12. The literature experimental conditions are $L = 3.66$ mm, $D = 152$ mm for Heskestad (1966), $L = 6$ mm, $D = 90$ mm for Tanaka and Tanaka (1976) and $L = 1.33$ mm, $D = 15.9$ mm for Witze and Dwyer (1976) with constrained radial jets; $L = 133$ mm, $D = 3$ mm for Witze and Dwyer (1976) with impinged radial jets. The normalized velocities decrease with the increasing normalized radial distance. The results can be fit as:

$$\frac{u_{r,m}}{u_{r,max}} = 1.26\left(\frac{r}{r_m}\right)^{-1.33}, \quad \text{for } r > 1.25r_m \tag{15}$$

The uncertainty in the calculation by Eq. (15) is 4.3%. It can be seen that the normalized velocities are inversely proportional to the 1.33th power of the normalized radial distance when $u_{r,m}$ and r_m are choose to be as the velocity scale and length scale. This is in agreement with theoretical derivation of Eq. (10). In Fig. 12, $r = 0$ is the virtual origin of the radial jet for all literature data. It can be seen that the current decay rate in this paper is greater than the constrained radial jet, and the current decay rate is lower than impinged radial jet when the radial distance is large enough.

Fig. 13 shows the relative turbulence intensities of the radial jet at impingement plane and the comparisons with the literature data from Witze and Dwyer (1976) and the free jet turbulence intensities data from Kwon and Seo (2005), Papanicolaou and List (1988). It can be seen that the data behave in nearly self-similar fashion when radial distance is small. The normalized turbulence intensities firstly decrease with the increasing radial distance, and they will reach minimum about 0.02 at about $r/D = 0.6$. Then the normalized turbulence intensities increase rapidly with the increasing radial distance until they reach the maximum at about $r/D = 5$. The normalized turbulence intensities will take constant values at $r/D > 5$. The normalized turbulence intensities increase slightly with the increasing normalized nozzle separations.

It also can be seen that the normalized turbulence intensities in this paper are larger than those produced by the constrained radial jet which take constant values about 0.3 at $r/D > 5$, and they are smaller than those produced by the impinged radial jet which take constant values about 0.6 at $r/D > 25$ (Witze and Dwyer, 1976). The normalized turbulence intensities produced by radial jet are also larger than that of free jet. Papanicolaou and List (1988) reported that the axial turbulent intensities of the free jet became constant 0.25 after about 50 diameters downstream, and Kwon and Seo (2005) reported that the axial turbulent intensities became constant of 0.22 after about 40 diameters downstream. This means the radial jet develops faster than the free jet.

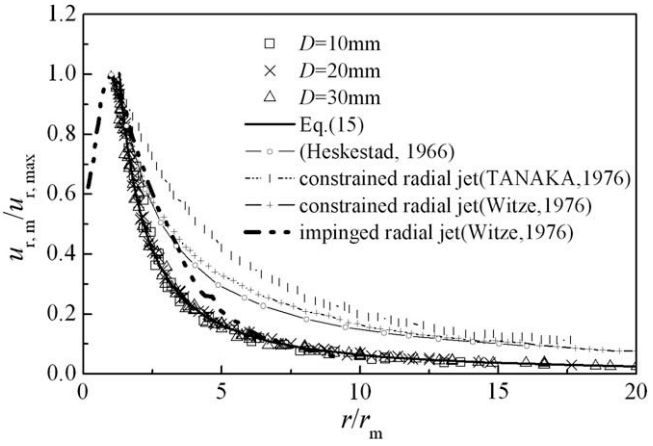

Fig. 12. The normalized radial velocity at impingement plane for $r > r_m$ ($u_0 = 23.6$ m/s).

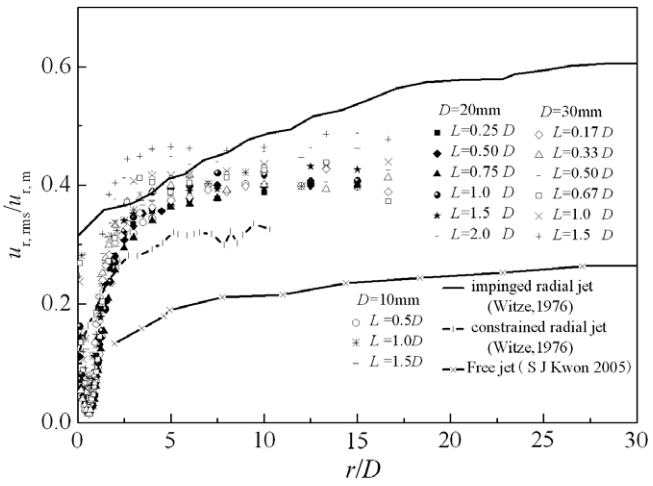

Fig. 13. The relative turbulence intensities at impingement plane.

4.4. The maximum radial velocity

The r_m at various nozzle diameters are shown in Fig. 14 when nozzle diameter is chosen to be length scale. From Fig. 14, it can be seen that, r_m increases with the nozzle separation at $L/D < 1$, and r_m keeps invariant at $L/D \geqslant 1$. This may be due to that, the pressure gradient in the impinging region is very large when the nozzle separation is small, which makes the exit air velocity asymmetric and forms double-peak structure just as mentioned in Korusoy and Whitelaw (2001). At small nozzle separations, the static pressure close to the nozzle is very high, which makes the fluid change direction as soon as they flow out from the nozzle. The static pressure close to the nozzle decreases with the increasing nozzle separations, and the fluid changing direction process becomes slower, so r_m increases. The exit air velocity becomes flatness and the double-peak structure almost disappears at $L/D \geqslant 1$ (Korusoy and Whitelaw, 2001), which indicates that the impinging region keeps invariant with the increasing nozzle separation at $L/D \geqslant 1$. So the nozzle separation has little influence on the fluid translation in impingement region, and r_m will keep invariant at $L/D \geqslant 1$.

From Fig. 14, it can be seen that, the difference of r_m/D is slightly at different nozzle diameters. The nozzle diameter and exit air velocity have little influence on r_m/D. r_m increases almost linearly with the increasing nozzle diameters. It perhaps because that the nozzle diameter has no influence on the flow structure at the same normalize nozzle separations.

The normalized maximum radial velocities at various nozzle diameters and exit air velocities are shown in Fig. 15. It can be

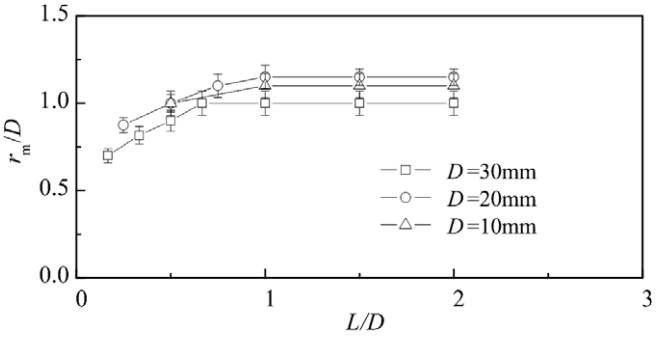

Fig. 14. The position of maximum radial velocity vs. normalized nozzle separation.

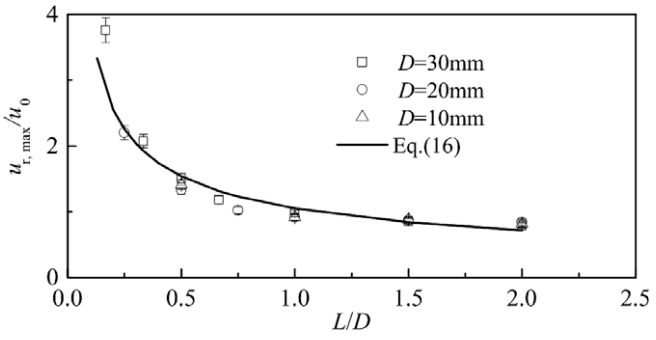

Fig. 15. The maximum radial velocity vs. normalized nozzle separation.

found that the normalized maximum radial velocities decrease with the increasing nozzle separations. The nozzle diameter and the exit air velocity have no influence on the normalized maximum radial velocities. The results can be fit as:

$$\frac{u_{r,m}}{u_0} = 1.05\left(\frac{L}{D}\right)^{-0.551}, \quad \text{for } 0.17 \leqslant L/D \leqslant 2. \tag{16}$$

The uncertainty in the calculation by Eq. (16) is 8.2%. It can be found that the maximum radial jet velocity at impingement plane is proportional to exit velocity, and it is inversely proportional to the 0.551th power of the normalized nozzle separation.

5. Conclusions

The radial velocities of the closely spaced opposed jets across various exit velocities, nozzle diameters and nozzle separations were studied experimentally by HWA and analyzed theoretically on the basis of N-S equation. The main conclusions can be summarized as follows:

The radial velocity distributions of the closely spaced opposed jets are self-similar across various sections, and they can be characterized as Gaussian distribution. The half-width is independent of exit velocity and nozzle diameters at $r > 1.5D$, and it increases slightly with the increasing normalized nozzle separations. The half-width increases linearly with the increasing radial distance, and its spreading rate is about 0.121 in this paper.

The normalized radial velocities are self-similar and only dependent on the normalized radial distance when $u_{r,max}$ and r_m are chosen to be the velocity scale and length scale, respectively. The normalized radial jet velocity is proportional to the normalized radial distance at $r < 0.78r_m$, but is inversely proportional to the 1.33th power of the normalized radial distance after at $r > 1.25r_m$. The normalized turbulence intensities are about 0.4 at $r/D > 5$ and $L/D \leqslant 1.0$.

The maximum radial jet velocity at impingement plane is proportional to exit velocity, and it is inversely proportional to the 0.551th power of the normalized nozzle separation. The position of the maximum radial jet velocity increases with the nozzle diameter; and it increases with the nozzle separation at $L/D < 1$, then it keeps invariant at $L/D \geqslant 1$.

Acknowledgments

This study was supported by the National Development Programming of Key Fundamental Researches of China (2010CB227004), National Natural Science Foundation of China (Grant No. 50776033), Program for Changjiang Scholars and Innovative Research Team in University (IRT0620) and New Century Excellent Talents in University (NCET-08-0775) by Ministry of Education of China.

References

Berman, Y., Tanklevsky, A., Oren, Y., Tamir, A., 2000. Modeling and experimental studies of SO_2 absorption in coaxial cylinders with impinging streams: part II. Chem. Eng. Sci. 55 (5), 1023–1038.
Bray, K.N.C., Champion, M., Libby, P.A., 1992. Premixed flames in stagnating turbulence. Part III. The turbulent kinetic energy and mean viscous dissipation (kappa–epsilon) theory for reactants impinging on a wall. Combust. Flame 91 (2), 165–186.
Champion, M., Libby, P.A., 1991. Asymptotic analysis of stagnating turbulent flows. AIAA J. 29 (1), 16–24.
Champion, M., Libby, P.A., 1993a. Comparison between theory and experiment for turbulence on opposed streams. Phys. Fluids 5 (9), 2301–2303.
Champion, M., Libby, P.A., 1993b. Reynolds stress description of opposed and impinging turbulent jets. Part I: closely spaced opposed jets. Phys. Fluids 5 (1), 203–216.
Dehkordi, A.M., 2002. Application of a novel opposed jets contacting device in liquid–liquid extraction. Chem. Eng. Process. 41 (3), 251–258.
Heskestad, G., 1966. Hot-wire measurements in a radial turbulent jet. J. Appl. Mech. Trans ASME 33, 417–424.
Hosseinalipour, S.M., Mujumda, A.S., 1995. Flow, heat transfer and particle drying characteristics in confined opposing turbulence jets: a numerical study. Drying Technol. 13 (3), 753–781.
Hunt, G.R., Ingham, D.B., 1992. The fluid mechanics of a two-dimensional Aaberg exhaust hood. Ann. Occup. Hyg. 36 (5), 455–476.
Hunt, G.R., Ingham, D.B., 1998. Laminar and turbulent radial jets. Acta Mech. 127 (1–4), 25–38.
Kawall, J.G., Shokr, M., Keffer, J.F., 1983. A digital technique for the simultaneous measurements of stream wise and lateral velocities in turbulent flows. J. Fluid Mech. 133, 83–122.
Korusoy, E., Whitelaw, J.H., 2001. Opposed jets with small separations and their implications for the extinction of opposed flames. Exp. Fluids 31 (1), 111–117.
Kostiuk, L.W., Bray, K.N.C., Cheng, R.K., 1993. Experimental study of premixed turbulent combustion in opposed streams part I. Nonreacting flow field. Combust. Flame 92 (4), 377–395.
Kwon, S.J., Seo, I.W., 2005. Reynolds number effects on the behavior of a non-buoyant round jet. Exp. Fluids 38 (6), 801–812.
Li, W.F., Sun, Z.G., Liu, H.F., Wang, F.C., Yu, Z.H., 2008. Experimental and numerical study on stagnation point offset of turbulent opposed jets. Chem. Eng. J. 138 (1–3), 283–294.
Lindstedt, R.P., Luff, D.S., Whitelaw, J.H., 2005. Velocity and strain-rate characteristics of opposed isothermal flows. Flow Turbul. Combust 74 (2), 169–194.
Papanicolaou, P.N., List, E.J., 1988. Investigations of round vertical turbulent buoyant jets. J. Fluid Mech. 195, 341–391.
Patel, R.P., 1979. Some measurements in radial free jets. AIAA J. 17 (6), 657–659.
Rajaratnam, N., 1976. Turbulent Jets. Elsevier. ISBN 0-444-41372-3.
Rubel, A., 1985. On the vortex stretching modification of the k–ε turbulence model: radial jets. AIAA J. 23 (7), 1129–1130.
Rumer, Y.B., 1949. Turbulent source of free annular jet. Dokl. Akad. Nauk SSSR 64, 463–466.
Santos, R.J., Teixeira, A.M., Lopes, J.C.B., 2005. Study of mixing and chemical reaction in RIM. Chem. Eng. Sci. 60 (8–9), 2381–2398.
Schwarz, W.H., 1963. The radial free jet. Chem. Eng. Sci. 18 (12), 779–786.
Stan, G., Johnson, D.A., 2001. Experimental and numerical analysis of turbulent opposed impinging jets. AIAA J. 39 (10), 1901–1908.
Tamir, A., 1994. Impinging-Stream Reactors: Fundamentals and Applications. Elsevier, Amsterdam.
Tanaka, T., Tanaka, E., 1976. Experimental study of a radial turbulent jet (1st report, effect of the nozzle shape on a free jet). Bull. JSME 19 (133), 792–799.
Wang, F.C., Zhoum, Z.J., Da, i.Z.G., et al., 2007. Development and demonstration plant operation of an opposed multi-burner coal–water slurry gasification technology. Energy Power Eng. China 1 (3), 251–258.
White, Frank M., 2004. Fluid Mechanics. McGraw-Hill, Columbus.
Witze, P.O., Dwyer, H.A., 1976. The turbulent radial jet. J. Fluid Mech. 75 (3), 401–417.
Wood, P.E., Chen, C.P., 1985. Turbulence model predictions of the radial jet—a comparison of k–ε models. Can. J. Chem. Eng. 63 (2), 177–182.